Estimates of crustal permeability on the Endeavour segment of the Juan de Fuca mid-ocean ridge

William S.D. Wilcock [a], Alex McNabb [b,1]

[a] *School of Oceanography, University of Washington, Seattle, WA 98195, USA*
[b] *Department of Mathematics, Massey University, Palmerston North, New Zealand*

Abstract

Observational studies of hydrothermal venting on the Endeavour segment of the Juan de Fuca Ridge place strong constraints on the spacing and area of vent fields, the depth of circulation, and the hydrothermal heat flux. A method is described to estimate a uniform crustal permeability from these parameters under the assumptions that upflow is confined to a narrow plume underlying each vent field and downflow can be described by potential flow into a point sink at the base of each plume. For a reasonable range of parameter values, the isotropic permeability of the Endeavour lies in the range 6×10^{-13} to 6×10^{-12} m^2. A significant elongation of vent fields along-axis suggests that the permeability structure is strongly anisotropic, with the across-axis permeability about an order of magnitude lower than the permeability in orthogonal directions.

Keywords: hydrothermal vents; permeability; Juan de Fuca Ridge; black smokers

1. Introduction

Hydrothermal circulation is the dominant mechanism for heat loss from young oceanic crust. High-temperature systems along mid-ocean ridges are characterized by the focused discharge of ~ 350°C fluids in black smoker vent fields. The physical laws governing porous convection are well known, but a full understanding of the configuration of circulation along mid-ocean ridges requires knowledge of the geometry of the heat source, the permeability of the medium, and the properties of the circulating fluids.

In recent years, seismic studies have greatly improved our understanding of the size and shape of magma chambers and of the thermal structure of young oceanic crust [1,2]. There has been considerable progress in characterizing the thermodynamic properties of the system $NaCl-H_2O$ at high temperatures and pressures [3], although this work has yet to be incorporated into convection calculations. In contrast, our knowledge of the permeability structure of young oceanic crust remains rather poor.

Direct determinations of the permeability of igneous oceanic crust are limited to laboratory studies of small samples or to single boreholes located well off-axis [4]. Since fluid fluxes are dominated by flow through larger cracks, measurements at small scales may not be representative of the large-scale perme-

---

[1] Present address: Division of Science and Technology, Tamaki Campus, University of Auckland, Auckland, New Zealand.

ability of fractured rocks. Downhole measurements at DSDP Hole 504B, which is located on heavily sedimented 6 My old crust on the Costa Rica rift, reveals basement permeabilities which decrease exponentially from 10^{-13}–10^{-14} m^2 in the upper 150 m to 10^{-15}–10^{-17} m^2, and less, at greater depths [4]. Models of topographically driven passive convection using these permeabilities have successfully predicted the observed patterns of seafloor heat flow in the region [5]. However, when these same permeabilities are included in axial convection calculations, the heat and mass fluxes from black smoker fields are severely underestimated [6]. As might be expected, the permeability is much higher in the extensional environment of the spreading axis. Experience in water-dominated geothermal fields shows that meaningful estimates of permeability in the field need to be obtained from kilometer scale measurements of pressure transients [7]. Such measurements are planned for the sedimented Middle Valley region of the Juan de Fuca Ridge, but it is unlikely that they will be obtained within young igneous crust for some time.

The most successful investigations of black smoker systems have employed pipe models [8–10] in which predefined recharge, heat uptake, and discharge zones are connected to form a single-pass system. These studies show that the high fluxes result from a combination of high permeabilities and a very thin conductive boundary layer between the heat source and the circulating fluid. Lowell and Burnell [9] estimate the product of the permeability and the thickness of the conductive boundary layer to be 5×10^{-12} m^3, while Lowell and Germanovich [10] estimate the permeability of upflow zones to be 3×10^{-13} to 3×10^{-11} m^2.

The Endeavour segment of the Juan de Fuca Ridge (Fig. 1) is the site of vigorous hydrothermal convection and has been subject to extensive studies which provide a unique set of constraints on the characteristics of circulation. The axial region of the Endeavour comprises a 100–150 m deep, 0.5–1 km wide, axial valley at a depth of 2200 m. Geological interpretations of SeaMARC I data [11] and submersible observations [12] show that the youngest extrusives are restricted to the valley floor, although the highly fissured and faulted appearance of the axial valley precludes very recent volcanism. Appar-
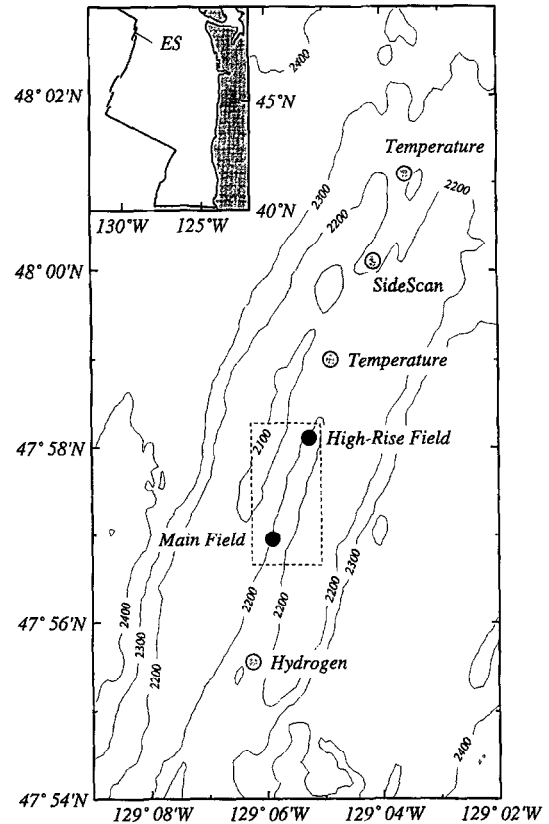
Fig. 1. Smoothed Seabeam bathymetry contoured at 100 m intervals showing the location of mapped vent fields (dots) [13,14] and possible venting sites (gray circles) inferred from temperature [16] and hydrogen [15] anomalies in the water column and from a high resolution side-scan sonar image [22]. The dashed box shows the area covered by Fig. 2. The inset map shows the location of Endeavour segment (ES) on the Juan de Fuca Ridge.

ently, ridge activity was formerly dominated by a volcanic phase, which has now been replaced by tectonic extension. Two vigorous vent fields, the Main and High-Rise fields (Figs. 1 and 2), lie 2 km apart, near the western wall of the axial valley, and have been mapped in detail [13,14]. Water column studies provide indirect evidence for at least three more fields spaced at regular intervals along-axis [13,15,16]. A large number of independent estimates have been made for the hydrothermal fluxes using both regional water column surveys [16–18] and local measurements in the Main vent field [16,19–21]. This paper is motivated by a desire to interpret the spacing and area of vent fields, the depth of
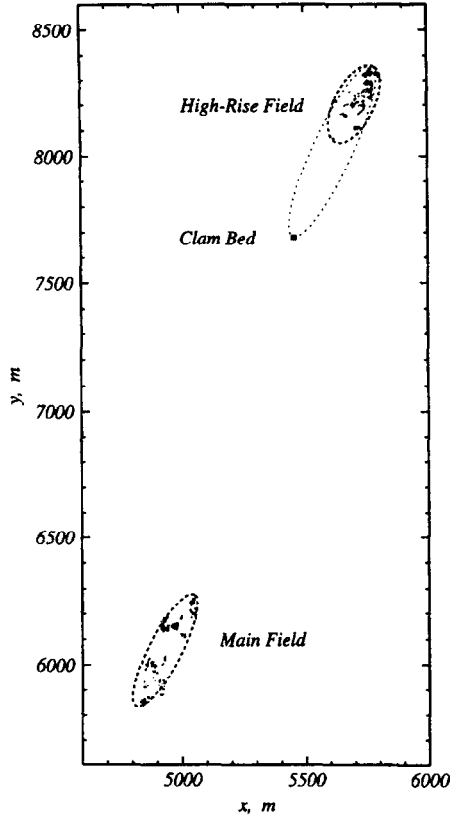
Fig. 2. Location of focused and diffuse venting structures in the Main and High-Rise vent fields [13,14]. The coordinate system is that of the transponder grid established during the 1988 dive program [13]. Dashed ellipses delimit the approximate dimensions of the vent fields. Clam Bed is a small venting structure [14] which may be an extension of the High-Rise field (dotted ellipse).

circulation, and the hydrothermal heat flux in terms of a uniform crustal permeability.

2. Method

Rather than employ a pipe model, we assume three-dimensional convection in an open system and seek simple solutions to approximate the upflow and downflow separately. If the upflow is confined to a plume of cross-sectional area A, which we equate to the area of the vent field, the mass flux, M, of venting fluids can be approximated by:

$$M = \frac{A\rho_h^k}{\mu_h}\left(\frac{\partial P_h'}{\partial z}\right) \qquad (1)$$

where ρ and μ are the density and viscosity of the fluid; subscript h refers to hot fluid; k is the vertical permeability; and z the depth below the seafloor. The quantity $\partial p_h'/\partial z$ is the deviation of the pressure gradient from the hydrostatic gradient for hot fluid and is related to the total pressure gradient, $\partial p/\partial z$, according to:

$$\frac{\partial p_h'}{\partial z} = \frac{\partial p}{\partial z} - \rho_h g \qquad (2)$$

where g is the acceleration of gravity. Because mid-ocean ridge vent fields are located on the floor of the axial valley rather than at shallower depths on the valley walls, topographic effects cannot play a significant role in controlling the configuration of these vigorous hydrothermal systems. For flat open-top systems, the horizontal pressure gradients are zero along the upper boundary and, if the permeability is uniform, can be taken as negligible in the near surface regions. This condition requires that:

$$\frac{\partial p_h'}{\partial z} - \frac{\partial p_c'}{\partial z} = g(\rho_c - \rho_h) \qquad (3)$$

where the subscript c refers to the properties of cold fluid. Because the dimensions of vent fields are small relative to their separation, we neglect the influence of upflow on downflow and model downflow by potential flow into a point sink at the base of each upflow zone. If the permeability is assumed to be homogeneous and isotropic, the pressure anomaly, p_c', created by a mass sink of strength $2M$ is:

$$p_c' = -\frac{M\mu_c}{2\pi\rho_c k}\frac{1}{r} \qquad (4)$$

where r is the distance from the sink. The flow we are seeking can be modeled by an infinite two-dimensional array of sinks (Fig. 3) of strength $(-1)^n 2M$ at coordinates $(mL, 0, (2n + 1)h)$, where L is the separation of vent fields, h is the depth of circulation, and m and n are integers. The resulting pressure field is:

$$p_c' = \frac{M\mu_c}{2\pi\rho_c k}\sum_{m=-\infty}^{\infty}\sum_{n=-\infty}^{\infty}$$

$$\times \frac{(-1)^n}{\left[(x - mL)^2 + y^2 + (z - (2n + 1)h)^2\right]^{1/2}} \qquad (5)$$

where x and y are measured along and across axis. At the origin, which corresponds the center of a vent field, the pressure gradient is:

$$\frac{\partial p}{\partial z} = \rho_c g \left[1 - X f(\alpha) \right] \qquad (6)$$

where:

$$X = \frac{M \mu_c}{2 \pi \rho_c^2 g k h^2} \qquad (7)$$

$$f(\alpha) = \sum_{m=-\infty}^{\infty} \sum_{n=-\infty}^{\infty} \frac{(-1)^n (2n+1)}{\left[\alpha^2 m^2 + (2n+1)^2 \right]^{3/2}} \qquad (8)$$

and:

$$\alpha = \frac{L}{h} \qquad (9)$$

The function $f(\alpha)$ is shown graphically in Fig. 4.
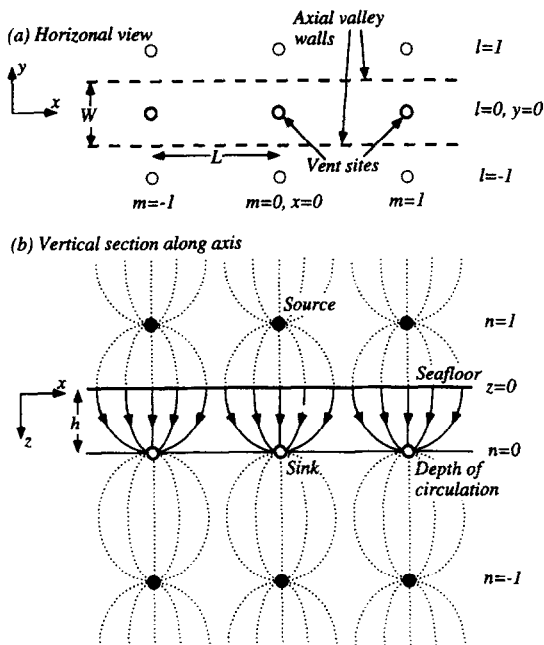
Fig. 3. (a) Horizontal and (b) vertical along-axis sections showing the configuration of the infinite array of sources (dots) and sinks (circles) used to model downflow (see text). Additional vertical planes of sinks (dotted circles) are required to confine downflow to the axial valley region.
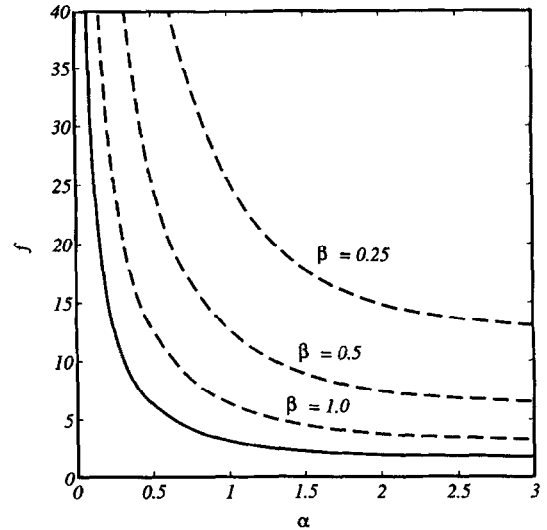
Fig. 4. Graph showing the function $f(\alpha)$ of Eq. (8) (solid line) and $f(\alpha,\beta)$ of Eq. (13) (dashed line) for $\beta = 0.25$, 0.5 and 1.

Substituting Eq. 6 into Eq. 2 yields an expression for the pressure gradient driving upflow:

$$\frac{\partial p_h'}{\partial z} = g \left[\rho_c - \rho_c X f(\alpha) - \rho_h \right] \qquad (10)$$

Substituting into Eq. 1 and solving for the permeability gives:

$$k = \frac{M \mu_h}{A \rho_h g (\rho_c - \rho_h)} (1 + fY) \qquad (11)$$

where:

$$Y = \frac{\mu_c}{\mu_h} \frac{\rho_h}{\rho_c} \frac{A}{2 \pi h^2} \qquad (12)$$

3. Observational constraints

The High-Rise vent field is located 2.2 km along axis, to the north of the Main vent field (Fig. 2), and there is indirect evidence for other significant venting sites spaced at similar distances to the north and south (Fig. 1). On the basis of potential temperature and light attenuation measurements in the water column, two possible new vent sites have been identified 4 and 8 km north of the Main vent field [16]. A strong hydrogen anomaly in the water column, 2.5 km south of the Main vent field [15], is probably

indicative of a venting source nearby. Delaney et al. [22] present a 120 kHz sidescan sonar map of the Endeavour which has sufficient resolution to identify sulfide structures. They report a region, 6 km to the north of the Main vent field, with the same textural characteristics as known vent fields. Cumulatively, these results suggests that vent fields on the Endeavour are spaced regularly, about 2 km apart.

Detailed maps of the Main and High-Rise vent fields [13,14] show that the position of individual vents coincide with faults and fissures which are aligned along axis. However, the vent fields are not limited to vents along a single fracture and it is possible to make a meaningful estimate of the field area. Active venting in the Main field [13] extends about 500 m along axis and 125 m across axis, while the High-Rise field [14] measures about 300 m by 150 m (Fig. 2). The average area of the fields is, thus, about 5×10^4 m^2. This simple picture of regularly spaced vent fields of uniform area is somewhat complicated by the existence of a small region of venting 500 m south of the High-Rise field, termed Clam Bed [14] (Fig. 2). Clam Bed may be an extension of the High-Rise field or it may be a small separate plume.

The depth of hydrothermal circulation cannot be determined directly from seafloor observations. Reaction zones inferred from quartz geobarometry and quartz–plagioclase geobarometry/geothermometry lie only a few hundred meters below the seafloor [23]. However, these depths are inconsistent with the lack of recent volcanic activity on the segment and the temperature and chemistry of venting fluids. Systematic spatial variations in fluid temperature and composition within the Main vent field apparently require supercritical phase separation [23], a result which implies fluids circulate to at least 1 km depth. A weak seismic reflector has been identified 2.5 km below the rise axis [24]. Tomographic inversions for the across-axis P wave velocity and attenuation structure [25,26] do not support the existence of a partially molten magma chamber beneath this reflector. Rather, the reflector lies at the base of zone of low velocities and high attenuation at 1–2 km depth, which is interpreted as a region of enhanced porosity [26]. It is conceivable that circulation extends to much greater depths, although the distribution of microearthquakes [27] provides no evidence that the axial region has cooled to large depths. Of 29 tectonic microearthquakes recorded over 2 weeks in 1991, none are constrained to lie beneath the axial valley. The seismic data and the characteristics of the venting fluids seem most compatible with a model in which circulation extends to a depth of about 2 km.

Three regional estimates of the heat flux from the Endeavour Segment have been obtained from surveys of the hydrothermal plumes that rise 100–300 m above the seafloor. Baker and Massoth [17] and Thomson et al. [16] employed tow-yo water column profiles to survey potential temperature anomalies within a region extending 10–15 km along-axis and used local current measurements to estimate the average heat anomaly being advected away from the vent sites. Baker and Massoth [17] report a heat flux of 1.7 ($\pm$1.1) $\times 10^9$ W from the Main and High Rise fields, although this is a minimum value, since the plume extended outside the western boundary of the survey area and the estimate does not account for the entrainment of colder deep water into the rising plume [28]. Thomson et al. [16] estimate a heat flux of 1.0 ($\pm$0.5) $\times 10^9$ W. Rosenberg et al. [18] used a ^{222}Rn radiogenic technique to calculate a heat flux of 3 ($\pm$2) $\times 10^9$ W for the Main field.

Thomson et al. [16] also present three estimates of the instantaneous flux being advected from the Main vent field. The fluxes range from 0.6 to 1.2 $\times 10^{10}$ W and are about an order of magnitude larger than the regional estimate obtained from the same data set. The reason for the discrepancy is unclear but the time-averaged regional estimates are probably more reliable [16]. Schultz et al. [19] measured the diffuse flux at a single location in the Main field. By extrapolating these measurements over the entire area of mapped sulfide structures, they infer that the total heat flux is dominated by diffuse flow and estimate a heat flux of 1 $\times 10^{10}$ W. Bemis et al. [20] and Ginster et al. [21] present individual measurements of the heat and mass fluxes from a large number of black smoker vents. By extrapolating their results to all known black smokers they estimate the black smoker heat flux to be 2–6 $\times 10^8$ W [20] and 3.6 ($\pm$0.7) $\times 10^8$ W [21] for the Main field and 1.2 ($\pm$0.6) $\times 10^8$ W [21] for the High-Rise field. By assuming that black smokers account for 6% of the total heat flux, Ginster et al. [21] estimate total heat fluxes of 6.1 ($\pm$1.3) $\times 10^9$ W and 2.0 ($\pm$1.0) $\times 10^9$

W for the Main and High-Rise fields, respectively. It is clear that all the heat flux estimates are accompanied by considerable uncertainty but, cumulatively, they show that the heat flux from the Main vent field lies in the range 10^9–10^{10} W, which is equivalent to a mass flux of 600–6000 kg s^{-1} of 350°C fluid.

4. Results

The observations discussed above lead us to assume values of $L = 2$ km, $h = 2$ km, $A = 5 \times 10^4$ m^2, and $M = 600$–6000 kg s^{-1} for our calculations. These values give $\alpha = 1.0$ and $f(\alpha) = 3.2$. Taking cold and hot fluid properties that are appropriate for temperatures of 0°C and 350°C ($\mu_c = 2 \times 10^{-3}$ Pa s, $\mu_h = 1 \times 10^{-4}$ Pa s, $\rho_c = 1030$ kg m^{-3}, $\rho_h = 700$ kg m^{-3}) Eq. 12 and (11) yield $Y = 0.028$ and a permeability estimate of 6×10^{-12} to 6×10^{-13} m^2. Physically, the product fY is the ratio of the magnitude of the pressure gradients driving downflow and upflow. The small value, $fY = 0.09$, implies that nearly all the available pressure gradient is driving upflow, a result that is in agreement with the inferences of other workers [10].

Sidescan sonar data [11,22] and submersible observations [12–14] show that the axial valley and its walls are highly fissured and faulted. It is reasonable to infer that the axial region may be a zone of enhanced permeability. To investigate the effect of limiting upflow to the axial valley, we assume that all the downflow is confined to a region of width W and, for simplicity, we assume the vents fields are centered in this region. The modified flow field is produced by extending the array of sources and sinks into three dimensions so that planes of sources and sinks are located at $y = lW$, where l is an integer. The new permeability estimate is given by Eq. 11 with f defined:

$$
f(\alpha,\beta) = \sum_{m=-\infty}^{\infty} \sum_{l=-\infty}^{\infty} \sum_{n=-\infty}^{\infty}
$$

$$
\times \frac{(-1)^n (2n+1)}{\left[\alpha^2 m^2 + \beta^2 l^2 + (2n+1)^2\right]^{3/2}}
$$

$$
(13)
$$

where:

$$
\beta = \frac{W}{h} \tag{14}
$$

The function $f(\alpha,\beta)$ is graphed in Fig. 4 for several values of β. The width of the axial valley and its walls is about 1 km, which gives $\beta = 0.5$, $f(\alpha,\beta) = 12.7$ (Fig. 4), and $fY = 0.35$. The estimated permeability increases only by about 25%.

The strong alignment of faults and fissure parallel to the ridge axis [11,22] and the existence of shallow crustal seismic anisotropy on the Juan de Fuca [29], lead to the inference that the permeability structure of the ridge axis may be strongly anisotropic with $k_{xx} \sim k_{zz} >> k_{yy}$. For the geometry of our model, fluid pressures in an anisotropic medium can be derived from isotropic solutions by rescaling along the principal axes of the permeability tensor [30] according to:

$$
x' = x\sqrt{\frac{k}{k_{xx}}} \; ; \quad y' = y\sqrt{\frac{k}{k_{yy}}} \; ; \quad z' = z\sqrt{\frac{k}{k_{zz}}}
$$

$$
(15)
$$

where (x',y',z') are the coordinates in the isotropic medium of permeability k, (x,y,z) the coordinates in the anisotropic medium, and it is assumed that the principal axes of the permeability tensor coincide with the axes of the coordinate system. We estimate the anisotropy of the Endeavour from the elongation of the vent fields. Symmetry considerations require that the upwelling plume assumes a circular cross section in an isotropic medium. For a horizontally anisotropic medium, the ratio of the along-axis to across-axis vent field dimensions will be given by $\sqrt{(k_{xx}/k_{yy})}$. The aspect ratio of the Main field is about 4, while that of the High-Rise field is 2 (Fig. 2). If Clam Bed is assumed to be an extension of the High Rise field, then the aspect ratio increases to 5. Thus, k_{xx}/k_{yy} appears to be ~ 10, a result that is independent of the absolute value of the permeability.

The permeability estimate of Eq. 11 has to be modified slightly in an anisotropic medium since, after rescaling the pressure field according to Eq. 15,

the strength of the sinks changes. Eq. 7 is replaced by:

$$X = \frac{M\mu_c}{2\pi\rho_c^2 g\sqrt{k_{xx}k_{yy}}\,h^2} \qquad (16)$$

and the solution for the permeability becomes:

$$k_{xx} = \frac{M\mu_h}{A\rho_h g(\rho_c - \rho_h)}\left(1 + \sqrt{\frac{k_{xx}}{k_{yy}}}\,fY\right) \qquad (17)$$

Taking $\sqrt{(k_{xx}/k_{yy})} = 2\text{–}5$, gives $fY\sqrt{(k_{xx}/k_{yy})} = 0.18\text{–}0.45$ for unconstrained downflow from which we estimate $k_{xx} = 6 \times 10^{-13}$ to 8×10^{-12} m^2 and $k_{yy} = 3 \times 10^{-14}$ to 2×10^{-12} m^2.

5. Discussion and conclusions

We have presented simple estimates for the permeability of the Endeavour segment of the Juan de Fuca Ridge, based on the assumptions that upflow occurs in regularly spaced plumes whose cross-sectional area is that of the vent field, and that downflow can be modeled by potential flow into a point sink at the base of each plume. This latter assumption works better for larger viscosity ratios μ_c/μ_h and higher Rayleigh numbers, since these favor small narrow regions of upflow which will have only a secondary effect on downflow. The Rayleigh number for hydrothermal convection is given by the expression:

$$Ra = \frac{\alpha_f g\,\rho_f^2 c_{pf} kh\,\Delta T}{\mu_f \lambda_m} \qquad (18)$$

where α is the volumetric coefficient of thermal expansion, c_p is the specific heat capacity, ΔT is the temperature change across the convecting region, λ is the conductivity, and subscripts f and m refer to properties of the fluid and to mean properties of the fluid and medium, respectively. Using properties for the fluid that are the intermediate between those of hot and cold fluid ($\alpha_f = 10^{-3}$°K^{-1}, $\rho_f = 850$ kg m^{-3}, $\mu_f = 450 \times 10^{-6}$ Pa s, $c_{pf} = 4000$ J kg^{-1}°K^{-1}), $\Delta T = 400$°K, $\lambda_m = 2$ W m^{-1}°K^{-1}, and our estimates for h and k yields $Ra \sim 10^4\text{–}10^5$. This high Rayleigh number is compatible with the vigorous nature of convection observed on the En-

deavour. Since high Rayleigh numbers are associated with high heat transport, thin thermal boundary layers, and narrow plumes, it is qualitatively compatible with our inference that the pressure gradients driving upflow exceed those driving downflow.

The permeability estimates are accompanied by significant uncertainties which arise both from uncertainties in the model parameters and from the simplifying assumptions behind our technique. The estimates of the heat and mass flux of hydrothermal fluids from the Endeavour differ by an order of magnitude which introduces an uncertainty factor of three to k. Because uncertainties in the depth of circulation and the spacing of plumes appear only in the product fY of Eq. 11, which is generally much less than unity, these quantities contribute only slightly to the uncertainty in k. For $fY \ll 1$, k is inversely proportional to the area of the upwelling plume. The location of vents is clearly controlled by the distribution of large surface fractures [13,14] and, so, the dimensions of the upwelling plume at depth may not correspond to the area delimited by active vents. In addition, a surface layer of high permeability can significantly focus upwelling [31].

For our model, a minimum estimate of the permeability can be obtained by assuming a cold hydrostatic pressure gradient in the upwelling plume (i.e., taking $fY = 0$). By modeling downflow by potential source into a point sink, as opposed to distributed sinks over the heat source at the base of the plume, we are probably overestimating the pressure gradients driving downflow and, hence, obtain a maximum value of the permeability. Because fY is small for all our calculations, the uncertainties inherent to analytical solutions is only 10–30%. However, much larger uncertainties will undoubtedly arise from the simplified geometry of the model and from our assumption of uniform permeability. These uncertainties are difficult to quantify.

In our model we implicitly assume that downflow is concentrated near the ridge axis. The chemistry of vent fluids on the Endeavour requires an organic source, which probably comes from sediments well off axis [32]. Heat flow data has been cited as evidence supporting recharge along the inward-facing faults which form the valleys flanking the axial valley [33]. Such a flow configuration would be better described by a pipe model. However, it is

unclear if either the chemical or heat flow data require more than a small proportion of the downflow to be located off axis. Spatial variations in the fluid temperatures and compositions in the Main vent field are most simply explained by a model in which downflow is concentrated between vent fields [34].

The thermodynamic and physical properties of water are very complex, particularly near the two-phase boundary, and the effects of two-phase separation on convection are poorly understood [35–37]. Clearly, more sophisticated numerical techniques are required to refine further our understanding of the constraints placed on the permeability structure by the extensive observations on the Endeavour. However, our study supports the inferences of other workers [8–10] that the permeability of young oceanic crust is high in the vicinity of black smoker fields.

Acknowledgements

References

[1] S.C. Solomon and D.R. Toomey, The structure of mid-ocean ridges, Annu. Rev. Earth Planet. Sci. 20, 329–364, 1992.

[2] J. Phipps Morgan, A. Harding, J. Orcutt, G. Kent and Y.J. Chen, An observational and theoretical synthesis of magma chamber geometry and crustal genesis along a mid-ocean ridge spreading center, in: Magmatic Systems, M.P. Ryan, ed., pp. 139–178, Academic Press, San Diego, CA, 1994.

[3] A. Anderko and K.S. Pitzer, Equation-of-state representation of phase equilibria and volumetric properties of the system $NaCl-H_2O$ above 573 K, Geochim. Cosmochim. Acta 57, 1657–1680, 1993.

[4] R.N. Anderson, M.D. Zoback, S.H. Hickman and R.L. New-

[5] A.T. Fisher, K. Becker, T.N. Narasimhan, M.G. Langseth and M.J. Mottl, Passive, off-axis convection through the southern flank of the Costa Rica rift, J. Geophys. Res. 95, 9343–9370, 1990.

[6] T. Brikowski and D. Norton, Influence of magma chamber geometry on hydrothermal activity at mid-ocean ridges, Earth Planet. Sci. Lett. 93, 241–255, 1989.

[7] M.A. Grant, I.G. Donaldson and P.F. Bixley, Geothermal Reservoir Engineering, 369 pp., Academic Press, New York, 1982.

[8] J.R. Cann, M.R. Strens and A. Rice, A simple magma-driven thermal balance model for the formation of volcanogenic massive sulphides, Earth Planet. Sci. Lett. 76, 123–134, 1985.

[9] R.P. Lowell and D.K. Burnell, Mathematical modeling of conductive heat transfer from a freezing, convecting magma chamber to a single-pass hydrothermal system: Implications for seafloor black smokers, Earth Planet. Sci. Lett. 104, 59–69, 1991.

[10] R.P. Lowell and L.N. Germanovich, On the temporal evolution of high-temperature hydrothermal systems at ocean ridge crests, J. Geophys. Res. 99, 565–575, 1994.

[11] E.S. Kappel and W.B.F. Ryan, Volcanic episodicity on a non-steady state rift valley along northeast Pacific spreading centers: Evidence from Sea MARC I, J. Geophys. Res. 91, 13,925–13,940, 1986.

[12] M.K. Tivey and J.R. Delaney, Growth of large sulfide structures on the Endeavour segment of the Juan de Fuca Ridge, Earth Planet. Sci. Lett. 77, 303–317, 1986.

[13] J.R. Delaney, V. Robigou, R.E. McDuff and M.K. Tivey, Geology of a vigorous hydrothermal system on the Endeavour segment, Juan de Fuca Ridge, J. Geophys. Res. 97, 19,663–19,682, 1992.

[14] V. Robigou, J.R. Delaney and D.S. Stakes, Large massive sulfide deposits in a newly discovered active hydrothermal system, the High-Rise field, Endeavour segment, Juan de Fuca Ridge, Geophys. Res. Lett. 20, 1887–1890, 1993.

[15] D.C. Kadko, N.D. Rosenberg, J.E. Lupton, R.W. Collier and M.D. Lilley, Chemical reaction rates and entrainment within the Endeavour Ridge hydrothermal plume, Earth Planet. Sci. Lett. 99, 315–335, 1990.

[16] R.E. Thomson, J.R. Delaney, R.E. McDuff, D.R. Janecky and J.S. McClain, Physical characteristics of the Endeavour Ridge hydrothermal plume during July 1988, Earth Planet. Sci. Lett. 111, 141–154, 1992.

[17] E.T. Baker and G.J. Massoth, Characteristics of hydrothermal plumes from two vent fields on the Juan de Fuca Ridge, northeast Pacific Ocean, Earth Planet. Sci. Lett. 85, 59–73, 1987.

[18] N.D. Rosenberg, J.E. Lupton, D. Kadko, R. Collier, M.D. Lilley and H. Pak, Estimation of heat and chemical fluxes from a seafloor hydrothermal vent field using radon measurements, Nature 334, 604–607, 1988.

[19] A. Schultz, J.R. Delaney and R.E. McDuff, On the partition-

ing of heat flux between diffuse and point source seafloor venting, J. Geophys. Res. 97, 12,299–12,314, 1992.

[20] K.G. Bemis, R.P. Von Herzen and M.J. Mottl, Geothermal heat flux from hydrothermal plumes on the Juan de Fuca Ridge, J. Geophys Res. 98, 6351–6365, 1993.

[21] U. Ginster, M.J. Mottl and R.P. Von Herzen, Heat flux from black smokers on the Endeavour and Cleft segments, Juan de Fuca Ridge, J. Geophys. Res. 99, 4937–4950, 1994.

[22] J.R. Delaney, R. McDuff, M. Lilley, R. Ballard, J.C. Sempéré, K. Stewart, V. Robigou, V. Atnipp, J. McClain, M. Holmes, D. Blackman and J. Howland, JASON/ALVIN operations on the Endeavour segment, Juan de Fuca Ridge — Summer 1991, EOS Trans. Am. Geopyhs. Union 72, 231, 1991.

[23] D.A. Butterfield, R.E. McDuff, M.J. Mottl, M.D. Lilley, J.E. Lupton and G.J. Massoth, Gradients in the composition of hydrothermal fluids from the Endeavour segment vent field: Phase separation and brine loss, J. Geophys. Res. 99, 9561–9583, 1994.

[24] K.M.M. Rohr, B. Milkereit and C.J. Yorath, Asymmetric deep crustal structure across the Juan de Fuca Ridge, Geology 16, 533–537, 1988.

[25] D.J. White and R.M. Clowes, Shallow crustal structure beneath the Juan de Fuca Ridge from 2-D seismic refraction tomography, Geophys. J. Int. 100, 349–367, 1990.

[26] D.J. White and R.M. Clowes, Seismic attenuation structure beneath the Juan de Fuca Ridge from tomographic inversion of amplitudes, J. Geophys. Res. 99, 3043–3056, 1994.

[27] J.S. McClain, M.L. Begnaud, M.A. Wright, J. Fondrk and G.K. Von Damm, Seismicity and tremor in a submarine hydrothermal field: The northern Juan de Fuca Ridge, Geophys. Res. Lett. 20, 1883–1886, 1993.

[28] E.T. Baker and S.R. Hammond, Hydrothermal venting and the apparent magmatic budget of the Juan de Fuca Ridge, J. Geophys. Res. 97, 3443–3456, 1992.

[29] M.A. McDonald, S.C. Webb, J.A. Hildebrand, B.D. Cornuelle and C.G. Fox, Seismic structure and anisotropy of the Juan de Fuca Ridge at 45°N, J. Geophys. Res. 99, 4857–4873, 1994.

[30] M. Muskat, The Flow of Homogeneous Fluids Through Porous Media, 763 pp., McGraw–Hill, New York, 1937.

[31] N.D. Rosenberg, F.J. Spera and R.M. Haymon, The relationship between flow and permeability field in seafloor hydrothermal systems, Earth Planet. Sci. Lett. 116, 135–153, 1993.

[32] M.D. Lilley, D.A. Butterfield, E.J. Olson, J.E. Lupton, S.A. Macko and R.E. McDuff, Anomalous CH_4 and NH_4^+ concentrations at an unsedimented mid-ocean ridge hydrothermal system, Nature 364, 45–47, 1993.

[33] H.P. Johnson, K. Becker and R. Von Herzen, Near-axis heat flow measurements on the northern Juan de Fuca Ridge: Implications for fluid circulation in oceanic crust, Geophys. Res. Lett. 20, 1875–1878, 1993.

[34] R.E. McDuff, J.R. Delaney, M.D. Lilley and D.A. Butterfield, Are up flow zones boundaries between adjacent hydrothermal systems?, EOS Trans. Am. Geophys. Union 75, 618, 1994.

[35] A. McNabb and J. Fenner, Thermohaline convection beneath the ocean floor, in: Proc. CSIRO/DSIR Seminar on Convective Flows in Porous Media, Wairakei, New Zealand, pp. 157–162, 1985.

[36] J.L. Bischoff and R.J. Rosenbauer, Salinity variations in submarine hydrothermal systems by layered double-diffusive convection, J. Geol. 97, 613–623, 1989.

[37] N.D. Rosenberg and F.J. Spera, Thermohaline convection in a porous medium heated from below, Int. J. Heat Mass Transfer 35, 1261–1273, 1992.